

Engraved hexagonal metamaterials resonators antenna for bio-implantable ISM-band applications

Belkheir Safaa¹, Sabri Ghoutia Naima²

¹Department of Electrical Engineering, Information Processing and Telecommunications Laboratory,
Faculty of Technology, University Tahri Mohammed, Bechar, Algeria

²Department of Material Sciences, Information Processing and Telecommunications Laboratory,
University Tahri Mohammed, Bechar, Algeria

Article Info

Article history:

Received May 13, 2024

Revised Oct 13, 2024

Accepted Oct 30, 2024

Keywords:

Antenna

Metamaterial

ISM

Hexagonal resonators

Engraving

ABSTRACT

This study will introduce a metamaterial antenna designing for use in biomedical implants. The antenna is compact and utilizes four slot complementary metamaterial hexagonal resonators of uniform shape and size. By incorporating the metamaterial into the antenna design, its size is reduced while the performance is enhanced. Simulation results show that the antenna achieves satisfactory peak gain values of -22.6 dBi and a 34.5% increase in bandwidth. Operating within the 2.4-2.5 GHz industrial, scientific, and medical (ISM) frequency bands, the antenna measures $7 \times 7 \times 1.27$ mm³ and consists of substrate layers with patch radiation, four metamaterials hexagonal resonators on the upper surface, a ground layer, and a second superstrate layer. The study also addresses the challenges and problems associated with the interaction between the antenna and human tissue, while aiming to maintain antenna performance, properties, and minimize its impact on tissues. Evaluation of when using a 2.45 GHz operating frequency, the specific absorption rate (SAR) shows values of 489.87 W/kg for 1 g of averaged tissue and 53.738 W/kg for 10 g of averaged tissue. The results of placing the antenna in human skin tissue are safe for use in the human body and appropriate for biomedical applications. Simulations conducted using computer simulation technology (CST) and high frequency structure simulator (HFSS) software emphasize the excellent performance of the engraved metamaterial antenna.

This is an open access article under the [CC BY-SA](https://creativecommons.org/licenses/by-sa/4.0/) license.



Corresponding Author:

Belkheir Safaa

Department of Electrical Engineering, Information Processing and Telecommunications Laboratory

Faculty of Technology, University Tahri Mohammed

08000 Bechar, Algeria

Email: belkheir.safaa@univ-bechar.dz

1. INTRODUCTION

With advancements in biomedical telemetry, there is a growing need for efficient, compact devices in medical applications. In recent years, there has been a growing research interest in implantable medical devices (IMDs). These devices are utilized in remote patient monitoring settings for tasks such as glucose monitoring, capsule endoscopy [1], [2], cardiac pacemakers [3], and intracranial pressure (ICP) monitoring.

IMDs utilize implantable antennas for bidirectional wireless communication [4], enabling the transmission of physiological data to receiving devices used by healthcare providers in Figure 1. However, designing these antennas presents several challenges [5]:

- Frequency range optimization.
- Miniaturization constraints.
- Tissue compatibility assurance.
- Implant safety protocols.
- Resonance shift mitigation.

The MICS band frequency, ranging from 402 to 405 MHz [6], [7], is utilized for implantable antennas in medical implant communication services. Additionally, industrial, scientific, and medical (ISM) bands cover frequency 2,400–2,500 MHz, 868–868.6 MHz, 902.8–928 MHz, and 433.1–434.8 MHz [8].

For implant these types of antennas we have to miniaturize these devices size, proposed a verity technique such as connecting the patch and ground by loading shorting pins [9], [10], a high dielectric constant material [11], metamaterial split ring resonator [12].

Metamaterials are called doubly negative materials (DNG), ($\epsilon < 0$ et $\mu < 0$) [13], [14], the beginning of the theoretical properties of this material was in 1986 by the scientist Veselago [15], in 2000, scientists [16], [17] successfully demonstrated the properties of metamaterials exhibiting both negative permeability and negative permittivity. Metamaterials have been used in many fields, and among the fields they have been applied to implantable antennas. Various miniaturization techniques for antennas have been documented in scientific literature [18], [19]. These techniques consist of:

- Employing metamaterial split ring resonators (SRRs).
- Utilizing complementary triangular ring resonators.
- Implementing complementary split ring resonators.
- Incorporating slots into patch antennas.
- Applying C-shaped slots.
- Using triangular electromagnetic resonators.
- Integrating complementary triangular electromagnetic resonators.

These approaches have demonstrated considerable potential for reducing antenna size while maintaining performance. Researchers are making significant strides in addressing these challenges. Recently, several antenna designs have been proposed for biotelemetry applications. Notably, scalp-implantable systems with integrated antennas were developed [20]. Initially, A $200 \times 200 \times 200$ mm³ homogeneous skin phantom (HSP) was used to model these antenna systems at a depth of 4 mm. Following measurement validation of the simulated results, gain values of -28.5 dBi at 915 MHz and -22.8 dBi at 2.45 GHz were obtained. Nonetheless, it was discovered that the specific absorption rate (SAR) for both frequencies was significantly high.

There has been an increase in interest in the application of metamaterials (MTMs) in implantable antenna design. With a gain of -25 dBi, researchers in reference [21] presented E-shaped and interdigital resonators appropriate for biomedical implant applications. In a similar vein, a different study suggested an antenna system with batteries, biosensors, and fake electronic parts in reference [22] to demonstrate the device architecture. This antenna's first simulations were carried out in a HSP that measured $150 \times 150 \times 150$ mm³, with a depth of 3 mm.

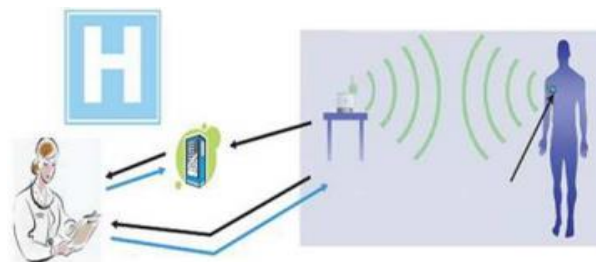


Figure 1. Health monitoring system [23]

In this paper, we provide a new metamaterial antenna design tailored specifically for medical applications, particularly in biotelemetry. This design is based on four complementary hexagonal metamaterial resonators etched into a patch. In open space, the suggested antenna was simulated, and through different human tissue layers, operating in the 2.4-2.5 GHz ISM band. Despite having dimensions comparable to previous designs, the proposed antenna exhibits superior performance, especially by achieving significantly lower SAR values than earlier models. A comparative performance analysis of the proposed design with recent studies is provided presented in Table 1.

Table 1. Comparing the proposed antenna with existing literature on the subject

Ref	Freq (GHz)	Size (mm)	Gain (dBi)	SAR 1g	SAR 10g
[20]	2.45	8×6×0.5	-22.8	807.34	102.04
[24]	2.45	11×11×1.27	-29	NAN	NAN
[25]	2.45	7×7×0.2	-22.29	591.40	82.71
[22]	2.45	12×12×0.635	-34	921	NAN
[21]	2.45	8×7×0.635	-25	758	80.1
[26]	2.45	8.2×6.94×0.75	-21.6	552	73.2
In this work	2.45	7×7×0.635	-20.32	489.87	53.738

2. DEVELOPMENT OF THE DESIGN

The process of antenna design evolution involves three main stages as illustrated in Figure 2, with a parametric analysis provided in Figure 3. In the first step, a basic rectangular patch is created with specific dimensions for the patch length (Lp) and patch width (Wp). The resonant frequency of the antenna at first 2.42 GHz with the return loss of -14.09 dB in antenna step 2 modifying patch form hexagonal the antenna’s resonant frequency at 2.5 GHz with the return loss of -21.75 dB However, the resonant frequency lies outside the intended ISM band range, the antenna’s resonant frequency is 2.43 GHz with the return loss of -26.71 dB New antenna design exhibits resonance near ISM frequencies, suitable for biometric application, the reflection of the antenna is not perfectly adapted. Therefore, an enhancement for the antenna is needed in bought terms size and elements, and for that we suggest using metamaterials.

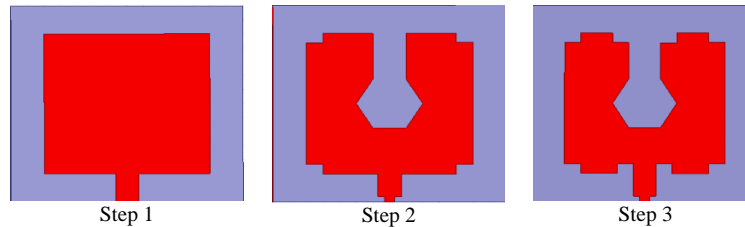


Figure 2. Evolution of design

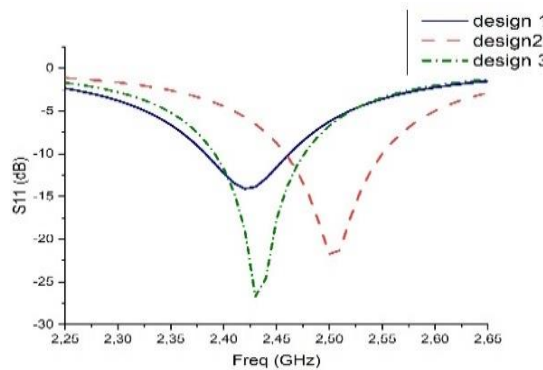


Figure 3. Return loss graph corresponding to three design of antenna

3. SIMULATION UNITE CELL METAMATERIAL

We simulate our hexagonal-shape resonator design with HFSS software, in X-axis boundary we applied along it the perfect electric conductor (PEC), and in Y-axis we applied along it the perfect magnetic conductor, and along Z-axis we have electromagnetic waves (port one and two) with perpendicular state to PEC and PMC, as shown in Figure 4. Figure 5 illustrates the transmission coefficient (S₂₁) and reflection coefficient (S₁₁) of the hexagonal-shaped resonator as a function of frequency.

The Nicolson ross weir (NRW) method is employed to determine if metamaterial characteristics are present in the proposed hexagonal resonators. This technique extracts the key parameters that define the behavior of the metamaterial (MTM), such as permeability, permittivity, and refractive index. The NRW method utilizes specific equations to calculate these parameters [21]-[27]:

$$V_I = S_{21} + S_{11} \tag{1}$$

$$V_2 = S_{21} - S_{11} \tag{2}$$

$$\mu_{eff} = \frac{2}{(jk_0 d)} \frac{(1 - V_2)}{(1 + V_2)} \tag{3}$$

$$\epsilon_{eff} = \frac{2}{(jk_0 d)} \frac{(1 - V_1)}{(1 + V_1)} \tag{4}$$

$$n = \sqrt{\mu_{eff} \times \epsilon_{eff}} \tag{5}$$

where:

- S_{11} , S_{21} the S-parameters coefficient (reflexion and transmission).
- Effective electromagnetic properties: ϵ_{eff} and μ_{eff} represent the effective permittivity and permeability, respectively, derived from S-parameter analysis.
- The wave number in free space is denoted as K_0 ($K_0 = \frac{\omega_0}{c}$), where C stands for the speed of light in free space (3×10^8 m/s) and ω_0 represents the angular frequency.
- d : The thickness of the substrate.

We confirmed the presence of the MTM effect in hexagonal resonators, and obtained the effective parameters illustrated in Figure 6. These include the real and imaginary parts of permittivity in Figure 6(a), permeability in Figure 6(b), and refractive index in Figure 6(c).

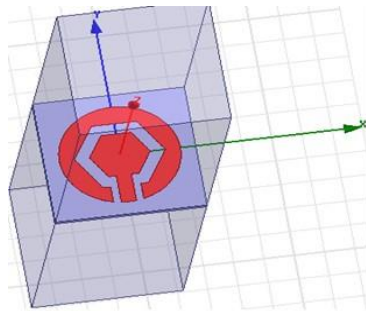


Figure 4. Proposed unit cell metamaterial

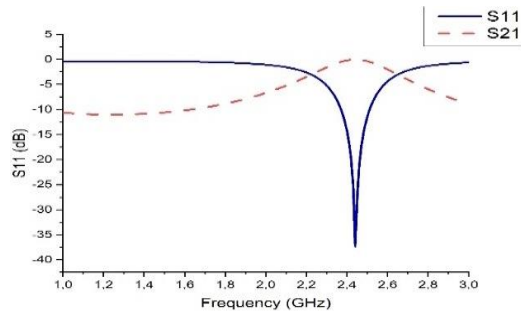


Figure 5. Displays the parameters S_{11} and S_{21}

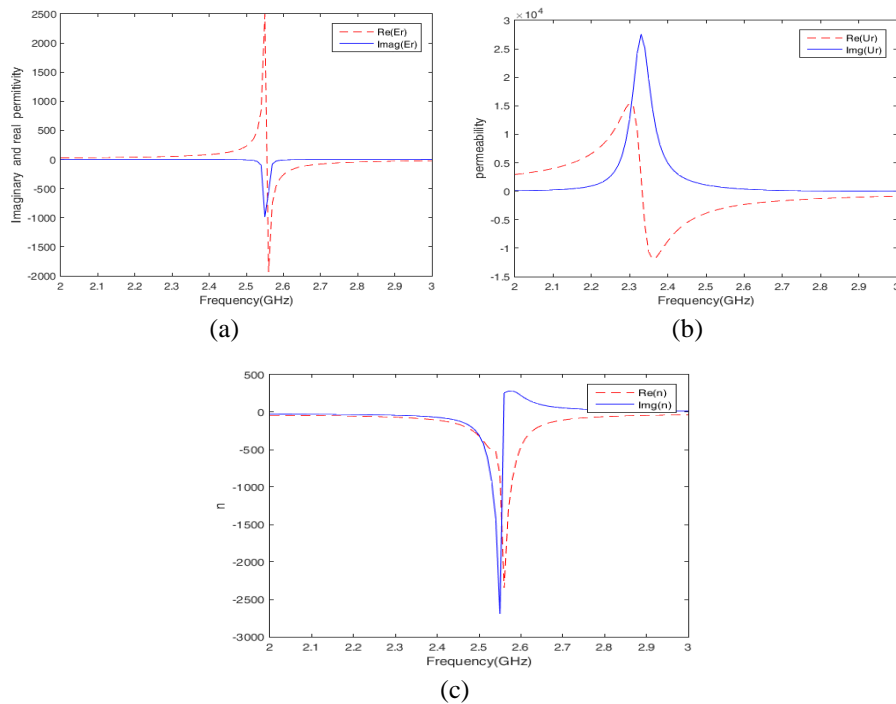


Figure 6. Effective parameters metamaterial: (a) permittivity, (b) permeability, and (c) refractive index

4. ANTENNA WITH FOUR HEXAGONAL RESONATORS

The conventional antenna is constructed using Rogers RO3210 substrate, which has a relative permittivity of $\epsilon_r=10.2$ and a thickness of $h=0.635$ mm. It consists of a first layer with a patch radiator and four MTM hexagonal-shaped resonators, along with a ground and a second superstrate layer. The antenna is connected by a coaxial cable with a shorting pin that measures 0.14 mm and 0.038 mm, respectively, and is intended to function at an impedance of 50 ohms. The antenna’s overall measurements, as shown in Figure 7, are $7 \times 7 \times 1.27$ mm³, and its resonance frequency is 2.45 GHz. A visual representation of the suggested metamaterial antenna can be found in Figure 7(a), while Figure 7(b) displays a side view of the developed antenna metamaterial structure, with the following parameter values: $W_g=7$ mm, $L_g=7$ mm, $L_p=5$ mm, $b=0.5$ mm, and $c=0.2$ mm.

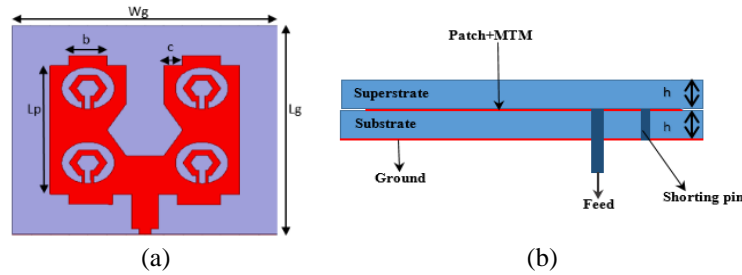


Figure 7. The proposed metamaterial antenna (a), (b) side viewed

5. SIMULATION ANTENNA METAMATERIAL IN FREE SPACE

Figure 8 illustrates the comparison of the reflection coefficient of the suggested antenna in free space both with and without the incorporation of the four hexagonal-shaped metamaterial. The simulation was conducted using two software applications, HFSS and CST. The results show a return loss value of approximately -26.7 dB and -28.47 dB without the metamaterial in HFSS and CST, respectively. When the four complementary metamaterials are added to the patch, the simulation indicates a return loss of -40.55 dB in HFSS and -31.1 dB in CST, exhibiting optimal return loss at the desired frequency within the ISM band. Presented in Table 2 the various values with a -10 dB bandwidth in open space.

Figure 9 presents a comparison of the far field gain patterns at 2.45 GHz, showing the antenna’s performance both with and without the addition of four MTM (metamaterial) resonators in an open environment. The comparison includes simulations for the E-plane (where $\phi = 0^\circ$) and the H-plane (where $\phi = 90^\circ$). These simulations were carried out using two different electromagnetic simulation software packages: HFSS and CST.

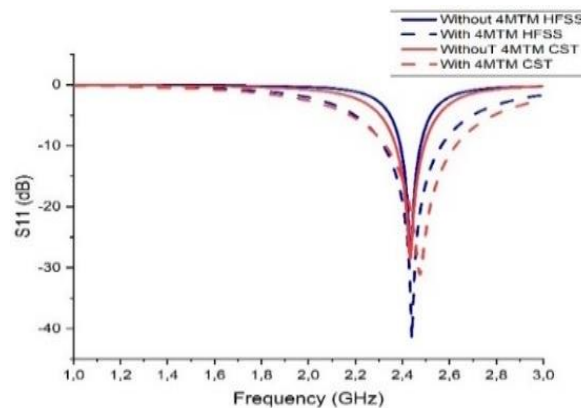


Figure 8. S-parameters in free space with frequency at 2.45 GHz

	HFSS (MHz)	CST (MHz)
Without 4 mtm	84.3	120.7
With 4 mtm	244.3	280.23

As seen in Figures 9(a) and (b), the suggested antenna shows a gain of roughly -29.3 dB at a frequency of 2.45 GHz in the two stimulators when the four hexagonal resonators are not present, the 2.45 GHz simulation results show peak gain values of -22.6 dB for the addition four MTM design in HFSS, as seen in Figure 9(c), and -23.6 dB in CST, as shown in Figure 9(d).

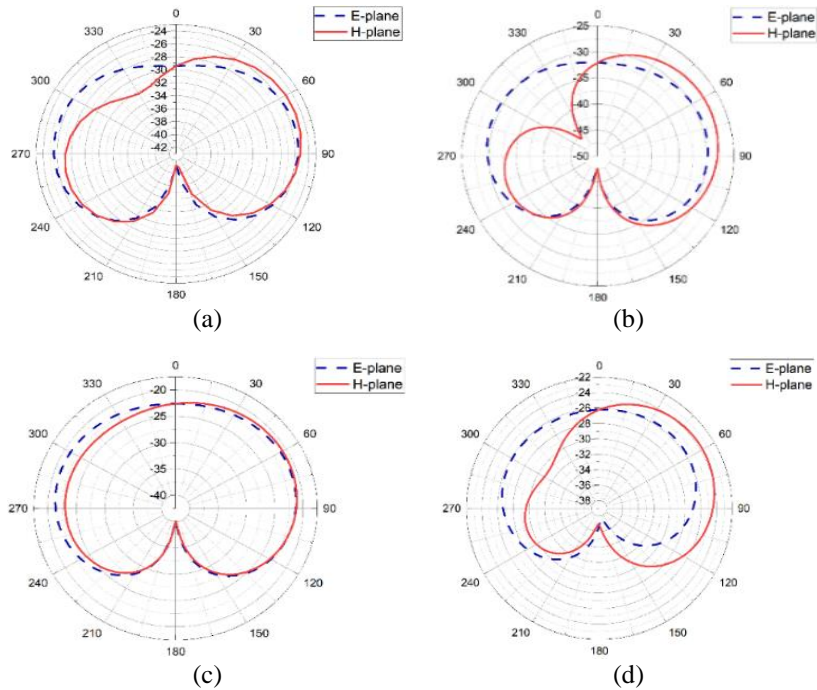


Figure 9. HFSS and CST software are used to compare the radiation pattern at 2.45 GHz in open space: Four MTM resonators are excluded in: (a)-(b) as opposed to four hexagonal-shaped resonators that are included in (c)-(d)

6. SIMULATION OF ANTENNAS IN SINGLE-LAYER AND THREE-LAYER TISSUE MODELS

As shown in Figure 10, we used two models to simulate the suggested metamaterial antenna in the second phase: a single-layer tissue and a three-layer tissue structure. Figure 10(a) illustrates the positioning of the metamaterial antenna on the skin model’s top layer. Figure 10(b) gives the three-layer model’s precise measurements. The tissue characteristics of skin ($\epsilon_r = 38, \sigma = 1.44 \text{ S/m}$), fat ($\epsilon_r = 5.28, \sigma = 0.2 \text{ S/m}$), and muscle ($\epsilon_r = 52.7, \sigma = 1.74 \text{ S/m}$) were used for the simulation at 2.45 GHz [21].

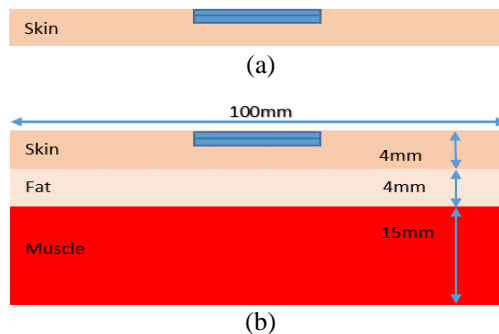


Figure 10. Both (a) single-layer and (b) three-layer tissue are used in the antenna

Figure 11 presents reflection coefficient simulations for the proposed antenna with MTM hexagonal shape:

- Figure 11(a) one-layer tissue model:
 - ✓ CST simulation: -27.29 dB return loss

- ✓ HFSS simulation: -32.81 dB return loss
- Figure 11(b) three-layer tissue model:
 - ✓ CST simulation: -13.6 dB return loss
 - ✓ HFSS simulation: -19.12 dB return loss"

Table 3 present's antenna metamaterial values with a -10 dB bandwidth, comparing single-layer (skin only) and three-layer (skin, fat, and muscle) human tissue models.

In Figure 12 illustrates the radiation gain for both the E and H planes in single-layer and three-layer tissue models, Figure 12 illustrates the bidirectional pattern of far field gain at 2.45 GHz the highest achieved gains are approximately -20.32 dB HFSS and -18.9 dB CST for a single layer, as shown in Figures 12(a) and 12(b) respectively. In the three-layer setup, the highest gains are recorded as -27.33 dB in HFSS and -21.1 dB in CST, shown in Figures 12(c) and 12(d) correspondingly.

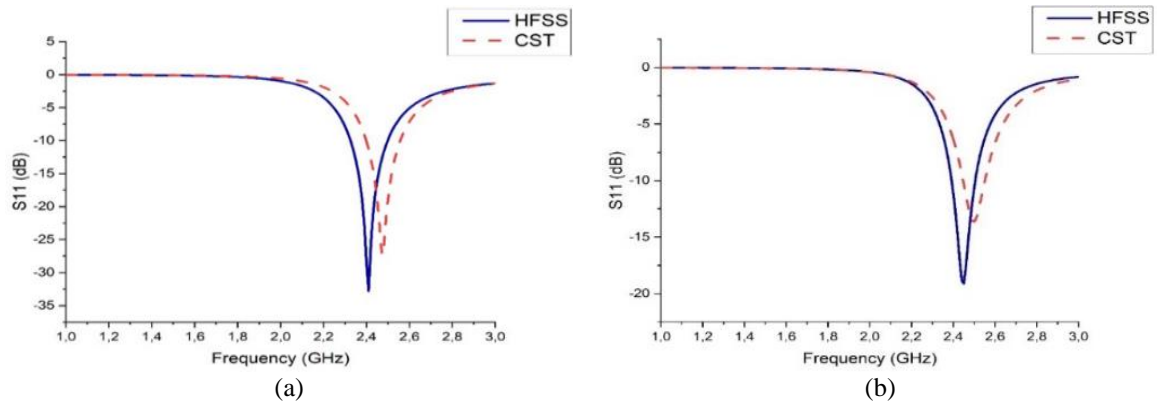


Figure 11. S-parameters (a) one layers tissues and (b) three layers tissues

Table 3. The bandwith value

	HFSS (MHz)	CST (MHz)-
One-layer model (MHz)	170.4	160.45
3-layers models (MHz)	111.5	105.83

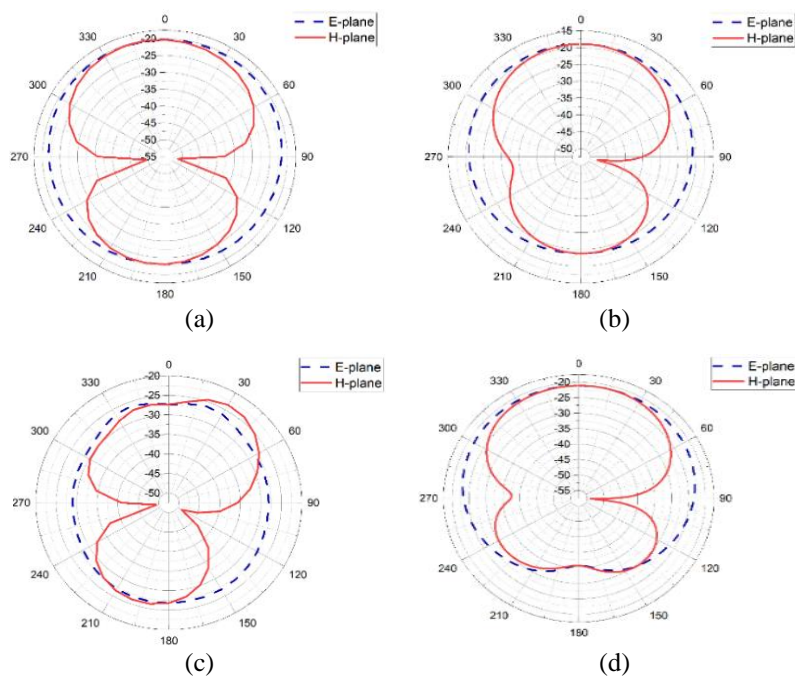


Figure 12. Radiation gain patterns at 2.45 GHz: (a)-(b) single-layer tissue model: E and H planes " (c)-(d) three-layer tissue model: E and H planes"

7. BIOCOMPATIBILITY AND SPECIFIC ABSORPTION RATE

To ensure patient safety, many implantable medical devices, such as antennas, need to be coated with biocompatible materials. If an implanted antenna comes in direct contact with metallization due to conductive human tissues, a short circuit can occur [28], [29]. Therefore, it is crucial to use biocompatible materials like Zirconia (ZrO_2) and Ceramic Alumina (Al_2O_3). The sensitivity of human tissues can be evaluated by measuring the electromagnetic radiation absorbed by a unit mass of these tissues, with the maximum acceptable limits set at $SAR_{1g} \leq 1.6$ W/Kg in the IEEE C95.1-1999 standard and $SAR_{10g} \leq 2$ W/Kg in the IEEE C95.1-2005 standard [30]. The SAR can be calculated using specific formulas [31], [32].

$$SAR = \frac{\sigma}{\rho} |E|^2 \tag{6}$$

Were:

- ρ the density of human tissue in kilograms per cubic meter (kg/m^3).
- σ the conductivity of the human tissue.
- E the electric field (V/m).

The SAR value is calculated in HFSS with reference power equal to 1 W and in CST with 0.5 W in one layer tissue (skin) at frequency 2.45 GHz using antenna with engraved MTM hexagonal resonator presented in Table 4.

The Figure 13 shows the distribution of SAR for MTM hexagonal resonator in skin layer obtained from HFSS and CST, respectively. In Figure 13(a), a simulation of the antenna’s impact on skin tissue using HFSS shows a reference power of 1 watt per 1g tissue mass, resulting in a value of 489.87 W/kg. Figure 13(b) displays a SAR simulation with the same power level but with 10g tissue mass, yielding a value of 53.738 W/kg. While Figure 13(c) represents simulations using CST, with a reference power of 0.5 watts in 1g tissue mass resulting in 8.11 W/kg, when, in Figure 13(d) with a 10 g tissue mass, the value is 3.49 W/kg, as we have seen in Table 4.

Table 4. Results SAR in 1 g and 10 g of one tissue (skin) in CST and HFSS

Masse of tissues	CST (0.5 W)		HFSS (1 W)	
	1 g-Avrg	10 g-Avrg	1 g-Avrg	10 g-Avrg
In this work	8.11	3.49	489.87	53.738

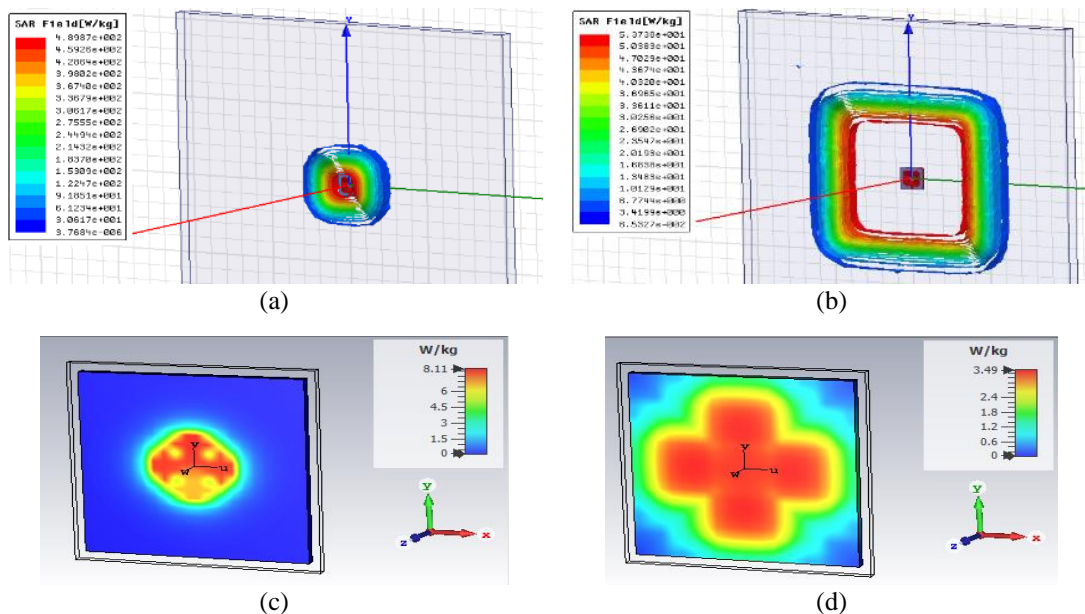


Figure 13. SAR distribution in the skin in HFSS: (a)-(b)1 g-10 g and CST (c)-(d) 1 g-10 g

The SAR values obtained in Table 4 and Figure 13 are unacceptable and harmful to human tissues, we adjusted the reference power level in order to maintain tissue integrity. To achieve standardized results, different power inputs were used for HFSS and CST simulations, as shown in Figure 14. HFSS simulations used a 3 mW input, while CST simulations used 2 mW. The resulting SAR distributions were as follows:

- For HFSS (3 mW reference power):
 - ✓ 1 g tissue mass: 1.46 W/kg Figure14(a).
 - ✓ 10 g tissue mass: 0.16 W/kg Figure14(b).
- For CST (2 mW reference power):
 - ✓ 1 g tissue mass: 1.2 W/kg Figure14(c).
 - ✓ 10 g tissue mass: 0.34 W/kg Figure14(d).

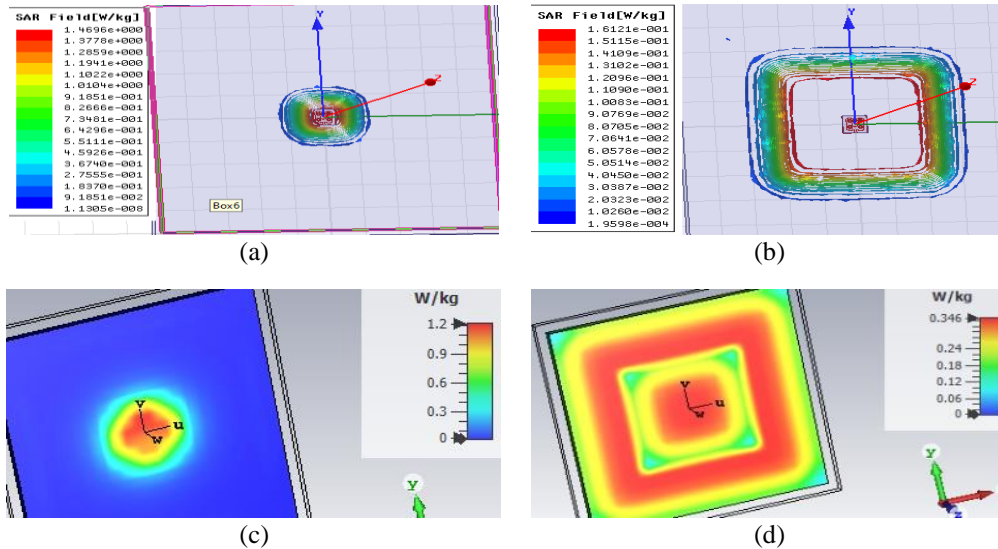


Figure 14. SAR distribution in the skin in HFSS: (a)-(b) 1 g-10 g and CST (c)-(d) 1 g-10 g

8. DISCUSSION

This study investigated the effects of integrating biocompatible antennas with metamaterials for implantable medical devices, while earlier research, such as the work by Shah and Yoo [20], explored the use of scalp-implantable antennas for monitoring intracranial pressure, these studies primarily focused on conventional antenna designs without addressing the potential benefits of metamaterial integration, specifically focusing on their performance in human tissue environments. Similarly, such as the work by Singh and Kaur [26], explored the design and testing of small footprint biocompatible antennas for implantable devices through in-silicon, in-vitro, and ex-vivo testing, they did not explicitly address the potential advantages of using metamaterials to enhance antenna efficiency and safety. Specifically, the impact of metamaterials on improving radiation performance and reducing SAR in complex tissue environments, such as multi-layered human tissues (skin, fat, and muscle), remains underexplored. This gap in the research highlights the need to investigate how metamaterials can optimize antenna performance while ensuring biocompatibility and safety for long-term medical applications.

We found that the integration of metamaterials with the antenna correlates with enhanced performance in terms of gain and bandwidth (mentioned in Figure 9 and Table 2). The proposed metamaterial-based antenna exhibited a significantly higher gain and broader bandwidth compared to conventional antennas. The variations in outcomes, encompassing primary beam strength, orientation, and breadth, can be attributed to the distinct algorithmic approaches utilized by HFSS and CST software packages. HFSS employs the FEM, or finite element method, which is generally considered more precise for antenna analysis. In contrast, CST implements the finite integration technique (FIT).

In previous studies, antennas simulated in human tissue typically showed lower maximum gain compared to free space simulations. This reduction was attributed to the antenna's small size relative to the human body and losses to the surrounding environment. However, the proposed antenna maintains its gain level even in tissue (Figure 12), which is a key achievement of this study, demonstrating its resilience to environmental changes. To ensure patient safety in real-world applications, we conducted simulations the SAR for our innovative implantable antenna, based on a 1-gram tissue average. When supplied with 1 watt of input power, the peak SAR values are computed, while elevated, remain below those reported for comparable devices in studies [20], [21]. However, to comply with the SAR limits outlined in IEEE C95.1: 1999, it's necessary to reduce the antenna's operating power to an appropriate level. The research focused on

developing an implantable antenna using metamaterials, and the gains resulted enhance the antenna in three parts:

- Significantly enhanced antenna performance and decrease the size.
- Maintained effectiveness despite environmental changes.
- Minimized impact on surrounding human tissue.

These outcomes directly addressed the primary objectives of the paper, ultimately leading to the successful design of an implantable antenna with improved characteristics. The integration of metamaterials in antenna design represents a significant advancement in biomedical applications. Our findings demonstrate that these antennas not only operate safely within human tissues but also effectively lower SAR levels, enhancing their suitability for therapeutic purposes while minimizing risks associated with energy absorption.

9. CONCLUSION

This article describes an antenna design featured four hexagonal-shaped resonators on the upper surface of a patch for biomedical telemetry. The antenna was simulated in free space using HFSS and CST software, resulted in a major enhancement in performances at a resonance frequency of 2.45 GHz with a high bandwidth of 244.8 MHz. Additionally, simulations were conducted in various tissues (skin, fat, and muscles) to assess the antenna's impact, with SAR values found to be within acceptable limits as outlined by IEEE C95.1:1999. The compact size and enhanced performance of the antenna make it suitable for use in implantable medical devices. Further research could explore the effects of implanting the antenna in different locations within a human body model to ensure compliance with safety standards for wireless medical devices.

ACKNOWLEDGEMENTS

This work is supported by Information Processing and Telecommunication Laboratory "LTIT". Finally, the authors of this work thank the anonymous reviewers for their careful reading and their insightful comments and suggestion.

REFERENCES

- [1] S. M. A. Shah, M. Zada, J. Nasir, O. Owais, A. Iqbal, and H. Yoo, "Miniaturized four-port MIMO Implantable antenna for high-data-rate wireless-capsule-endoscopy applications," *IEEE Transactions on Antennas and Propagation*, vol. 71, no. 4, pp. 3123–3133, Apr. 2023, doi: 10.1109/TAP.2023.3243984.
- [2] G. Wang, X. Xuan, D. Jiang, K. Li, and W. Wang, "A miniaturized implantable antenna sensor for wireless capsule endoscopy system," *AEU - International Journal of Electronics and Communications*, vol. 143, p. 154022, Jan. 2022, doi: 10.1016/j.aeue.2021.154022.
- [3] M. Wang *et al.*, "Broadband implantable antenna for wireless power transfer in cardiac pacemaker applications," *IEEE Journal of Electromagnetics, RF and Microwaves in Medicine and Biology*, vol. 5, no. 1, pp. 2–8, 2021, doi: 10.1109/JERM.2020.2999205.
- [4] C. Liu, Y.-X. Guo, and S. Xiao, "Capacitively loaded circularly polarized implantable patch antenna for ISM band biomedical applications," *IEEE Transactions on Antennas and Propagation*, vol. 62, no. 5, pp. 2407–2417, 2014, doi: 10.1109/TAP.2014.2307341.
- [5] A. Kiourti, J. R. Costa, C. A. Fernandes, A. G. Santiago, and K. S. Nikita, "Miniature implantable antennas for biomedical telemetry: from simulation to realization," *IEEE Transactions on Biomedical Engineering*, vol. 59, no. 11, pp. 3140–3147, Nov. 2012, doi: 10.1109/TBME.2012.2202659.
- [6] Li-Jie Xu, Yong-Xin Guo, and Wen Wu, "Miniaturized dual-band antenna for implantable wireless communications," *IEEE Antennas and Wireless Propagation Letters*, vol. 13, pp. 1160–1163, 2014, doi: 10.1109/LAWP.2014.2329937.
- [7] L.-J. Xu, Y.-X. Guo, and W. Wu, "Bandwidth enhancement of an implantable antenna," *IEEE Antennas and Wireless Propagation Letters*, vol. 14, pp. 1510–1513, 2015, doi: 10.1109/LAWP.2014.2374217.
- [8] A. Kiourti and K. S. Nikita, "Miniature scalp-implantable antennas for telemetry in the MICS and ISM bands: design, safety considerations and link budget analysis," *IEEE Transactions on Antennas and Propagation*, vol. 60, no. 8, pp. 3568–3575, Aug. 2012, doi: 10.1109/TAP.2012.2201078.
- [9] R. Waterhouse, "Small microstrip patch antenna," *Electronics Letters*, vol. 31, no. 8, pp. 604–605, 1995, doi: 10.1049/el:19950426.
- [10] C. Liu, Y.-X. Guo, H. Sun, and S. Xiao, "Design and safety considerations of an implantable rectenna for far-field wireless power transfer," *IEEE Transactions on Antennas and Propagation*, vol. 62, no. 11, pp. 5798–5806, Nov. 2014, doi: 10.1109/TAP.2014.2352363.
- [11] J. Kim and Y. Rahmat-Samii, "Implanted antennas inside a human body: simulations, designs, and characterizations," *IEEE Transactions on Microwave Theory and Techniques*, vol. 52, no. 8, pp. 1934–1943, 2004, doi: 10.1109/TMTT.2004.832018.
- [12] T. Ali and R. C. Biradar, "A compact multiband antenna using $\lambda/4$ rectangular stub loaded with metamaterial for IEEE 802.11N and IEEE 802.16E," *Microwave and Optical Technology Letters*, vol. 59, no. 5, pp. 1000–1006, 2017, doi: 10.1002/mop.30454.
- [13] J. P. Barrett and S. A. Cummer, "Design and full characterization of planar active magnetic RF metamaterials," *IEEE Antennas and Wireless Propagation Letters*, vol. 14, pp. 943–946, Dec. 2015, doi: 10.1109/LAWP.2014.2388431.
- [14] K. Becharef, K. Nouri, H. Kandouci, B. S. Bouazza, M. Damou, and T. H. C. Bouazza, "Design and simulation of a broadband bandpass filter based on complementary split ring resonator circular 'CSRRs,'" *Wireless Personal Communications*, vol. 111, no. 3, pp. 1341–1354, Apr. 2020, doi: 10.1007/s11277-019-06918-6.
- [15] V. G. Veselago, "The electrodynamics of substances with simultaneously negative values of ϵ and μ ," *Soviet Physics Uspekhi*, vol. 10, no. 4, pp. 509–514, Apr. 1968, doi: 10.1070/PU1968v010n04ABEH003699.

- [16] J. B. Pendry, A. J. Holden, D. J. Robbins, and W. J. Stewart, "Low frequency plasmons in thin-wire structures," *Journal of Physics: Condensed Matter*, vol. 10, no. 22, pp. 4785–4809, Jun. 1998, doi: 10.1088/0953-8984/10/22/007.
- [17] D. R. Smith, D. C. Vier, N. Kroll, and S. Schultz, "Direct calculation of permeability and permittivity for a left-handed metamaterial," *Applied Physics Letters*, vol. 77, no. 14, pp. 2246–2248, Oct. 2000, doi: 10.1063/1.1314884.
- [18] C. Zhu *et al.*, "Electrically small metamaterial-inspired tri-band antenna with meta-mode," *IEEE Antennas and Wireless Propagation Letters*, vol. 14, pp. 1738–1741, 2015, doi: 10.1109/LAWP.2015.2421356.
- [19] S. Bhattacharjee, S. Maity, S. R. Bhadra Chaudhuri, and M. Mitra, "Metamaterial-inspired wideband biocompatible antenna for implantable applications," *IET Microwaves, Antennas & Propagation*, vol. 12, no. 11, pp. 1799–1805, Sep. 2018, doi: 10.1049/iet-map.2017.1143.
- [20] S. A. A. Shah and H. Yoo, "Scalp-implantable antenna systems for intracranial pressure monitoring," *IEEE Transactions on Antennas and Propagation*, vol. 66, no. 4, pp. 2170–2173, 2018, doi: 10.1109/TAP.2018.2801346.
- [21] A. Saidi, K. Nouri, B. S. Bouazza, K. Becharef, A. Cherifi, and T. Abes, "E-shape metamaterials embedded implantable antenna for ISM-band biomedical applications," *Research on Biomedical Engineering*, vol. 38, no. 2, pp. 351–368, Apr. 26, 2022, doi: 10.1007/s42600-021-00191-y.
- [22] M. Wang *et al.*, "Broadband implantable antenna for wireless power transfer in cardiac pacemaker applications," *IEEE Journal of Electromagnetics, RF and Microwaves in Medicine and Biology*, vol. 5, no. 1, pp. 2–8, 2021, doi: 10.1109/JERM.2020.2999205.
- [23] N. A. Malik, P. Sant, T. Ajmal, and M. Ur-Rehman, "Implantable antennas for bio-medical applications," *IEEE Journal of Electromagnetics, RF and Microwaves in Medicine and Biology*, vol. 5, no. 1, pp. 84–96, 2021, doi: 10.1109/JERM.2020.3026588.
- [24] C. Liu, Y. Zhang, and X. Liu, "Circularly polarized implantable antenna for 915 MHz ISM-band far-field wireless power transmission," *IEEE Antennas and Wireless Propagation Letters*, vol. 17, no. 3, pp. 373–376, 2018, doi: 10.1109/LAWP.2018.2790418.
- [25] F. Faisal, M. Zada, A. Ejaz, Y. Amin, S. Ullah, and H. Yoo, "A miniaturized dual-band implantable antenna system for medical applications," *IEEE Transactions on Antennas and Propagation*, vol. 68, no. 2, pp. 1161–1165, 2020, doi: 10.1109/TAP.2019.2938591.
- [26] G. Singh and J. Kaur, "Small footprint biocompatible antenna for implantable devices: design, in-silico, in-vitro and ex-vivo testing," *Iranian Journal of Science and Technology, Transactions of Electrical Engineering*, vol. 47, no. 3, pp. 1145–1152, Sep. 2023, doi: 10.1007/s40998-023-00588-8.
- [27] P. C. Paul, M. J. Hossain, A. K. Karmaker, and M. J. Islam, "A new double u-shaped compact negative refractive index metamaterial for wideband applications," *Indonesian Journal of Electrical Engineering and Computer Science*, vol. 20, no. 2, pp. 863–869, 2020, doi: 10.11591/ijeecs.v20.i2.pp863-869.
- [28] M. M. Ali, M. E. I. Bashar, and M. K. Hosain, "Circular planner inverted-f antenna for implantable biomedical applications," in *2017 2nd International Conference on Electrical & Electronic Engineering (ICEEE)*, 2017, pp. 1–4, doi: 10.1109/ICEEE.2017.8412844.
- [29] A. O. Kaka, M. Toyacan, and S. D. Walker, "Miniaturized stacked implant antenna design at ISM band with biocompatible characteristics," *COMPEL: The International Journal for Computation and Mathematics in Electrical and Electronic Engineering*, vol. 34, no. 4, pp. 1270–1285, Jul. 2015, doi: 10.1108/COMPEL-02-2015-0032.
- [30] B. P. Nadh, B. T. P. Madhav, and M. S. Kumar, "Design and analysis of dual band implantable DGS antenna for medical applications," *Sādhanā*, vol. 44, no. 6, p. 131, Jun. 2019, doi: 10.1007/s12046-019-1099-8.
- [31] W. H. Bailey *et al.*, "Synopsis of IEEE Std C95.1™-2019 'IEEE standard for safety levels with respect to human exposure to electric, magnetic, and electromagnetic fields, 0 Hz to 300 GHz,'" *IEEE Access*, vol. 7, pp. 171346–171356, 2019, doi: 10.1109/ACCESS.2019.2954823.
- [32] S. Bhattacharjee, S. Maity, S. R. Bhadra Chaudhuri, and M. Mitra, "Metamaterial-inspired wideband biocompatible antenna for implantable applications," *IET Microwaves, Antennas & Propagation*, vol. 12, no. 11, pp. 1799–1805, Sep. 2018, doi: 10.1049/iet-map.2017.1143.

BIOGRAPHIES OF AUTHORS



Belkheir Safaa    received the Licence and Master degrees from the University Tahri Mohammed Bechar, Algeria, in 2018 and 2021, respectively, in telecommunication, and telecommunication systems. Currently continuing studies to obtain the Ph.D. degree in telecommunication systems at Department of Electrical Engineering at the University Tahri Mohamed Bechar. The research focuses on metamaterials. She can be contacted at email: belkheir.safaa@univ-bechar.dz.



Sabri Ghoutia Naima    was born in Tlemcen and she has obtained her Doctorate degrees from University of Tlemcen since 2010 in Electronics-Physics. Actually, she is Professor at university of Tahri Mohamed, Bechar. Her scientific fields of interest are: Materials and metamaterials for optical and microwave devices, optical networks and telecommunications systems, microwaves, optical transmission, and laser DBR. She can be contacted at email: sabri.ghoutia@univ-bechar.dz.